A 40-Gb/s/ch WDM Transmission with SPM/XPM Suppression Through Prechirping and Dispersion Management

Akihide Sano, Yutaka Miyamoto, *Member, IEEE*, Shoichiro Kuwahara, and Hiromu Toba, *Member, IEEE*

***Abstract*—This paper proposes to combine prechirping with dispersion management scheme in such a way as to suppress the power penalty induced by self-phase modulation (SPM) and cross-phase modulation (XPM) in 40-Gb/s per channel wavelength-division multiplexed (WDM) transmission systems with long-amplifier spacing. First, we show that the optimum total dispersion to minimize SPM depends on prechirping and the local dispersion of the transmission fiber, unlike that for minimizing XPM. Next, it is shown that, by optimizing the combination of prechirping and local dispersion, these two optima can be made to match so as to improve the allowable maximum fiber input power. Finally, the operation of the proposed optimization scheme is confirmed experimentally, and 4 $\times$ 40-Gb/s WDM transmission over 400 km of nonzero dispersion-shifted fiber (NZDSF) is demonstrated successfully with the fiber input power of $+10$ dBm/ch and 250 GHz channel spacing.**

***Index Terms*—Cross-phase modulation (XPM), dispersion management, optical fiber transmission, prechirping, self-phase modulation, wavelength-division multiplexing (WDM).**

I. Introduction

LARGE capacity wavelength-division multiplexed (WDM) transmission systems based on high-speed time-division multiplexing (TDM) technology are attractive because of their high spectral efficiency, reduced system size, and support of network management. Up to now, 10 Gb/s systems have been already installed in the field. Recently, the line rate of 40 Gb/s has been achieved by electrical TDM (ETDM) technology [1]–[4]. Moreover, 40 Gb/s per channel WDM transmission experiments based on ETDM technology with total capacities over 1 Tbit/s have conducted by several groups [5]–[7].

In terrestrial systems, from the viewpoints of cost and network management, it is desirable that 40-Gb/s systems offer the same amplifier spacing as that of existing 10-Gb/s systems. For this reason, higher fiber input power is required in 40-Gb/s systems compared to the lower bit rate systems. However, nonlinear optical effects such as self-phase modulation (SPM), cross-phase modulation (XPM) and four-wave mixing (FWM) limit the fiber input power. Dispersion management, which employs dispersion compensation and dispersive transmission fibers such as standard single mode fibers (SMF), nonzero dispersion- shifted fibers (NZDSF), and dispersion-shifted fibers with L-band signal, effectively suppresses the FWM degradation. When these fibers are used, SPM and XPM cause serious waveform distortion in conjunction with the fiber group velocity dispersion (GVD). It is known that SMF is stronger against XPM because of its large effective area and high local dispersion in the gain band of erbium-doped fiber amplifiers (EDFA) [8]. The use of NZDSF, on the other hand, reduces the required total dispersion of the dispersion compensators thanks to its lower dispersion. NZDSF also offers the option of Raman amplification with relatively high efficiency [5]. In the case of NZDSF transmission, however, the sign of the local dispersion affects the transmission characteristics in conjunction with SPM [9]. Therefore, suppressing the SPM-GVD interaction and XPM-GVD interaction is an important issue to realize 40-Gb/s-based WDM systems using NZDSF.

Prechirping is known to reduce the power penalty induced by fiber nonlinearity both in normal and anomalous dispersion fibers [10]–[12]. In this paper, we propose that the combination of dispersion management and prechirping should be optimized in order to suppress both SPM- and XPM-induced waveform distortion for 40-Gb/s/ch WDM systems using NZDSF. Section II discusses the dependence of the optimum total dispersion for SPM and that for XPM on initial chirping and local dispersion of the fiber, and describes the operation principle of the proposed scheme. Sections III and IV theoretically examine the power penalty caused by SPM and XPM, respectively, and show that the proposed suppression scheme effectively increases the allowable fiber input power. In Section V, the operation of the proposed scheme is experimentally confirmed in 4 $\times$ 40-Gb/s 400-km transmission with the average fiber input power of $+10$ dBm/channel and the channel spacing of 250 GHz.

II. Operation Principle

Because the refractive index in the transmission fiber changes with the intensity of the transmitted signal, the signal suffers phase modulation (SPM and XPM). SPM is caused by intensity modulation of the target channel, and XPM results from intensity modulation of the other copropagating WDM channels. Although these effects are converted into intensity modulation through the interaction with GVD and cause waveform distortion, this waveform distortion can be suppressed to a certain extent by adjusting the total dispersion to zero at the end

Manuscript received April 14, 2000; revised August 16, 2000.

A. Sano was with NTT Network Innovation Laboratories, Kanagawa, 239-0847 Japan. He is now with NTT Network Service Systems Laboratories, 3-9-11, Tokyo, 180-8585, Japan (e-mail: sano.akihide@lab.ntt.co.jp).

Y. Miyamoto, S. Kuwahara, and H. Toba are with NTT Network Innovation Laboratories, Kanagawa, 239-0847, Japan.

Publisher Item Identifier S 0733-8724(00)09827-3.

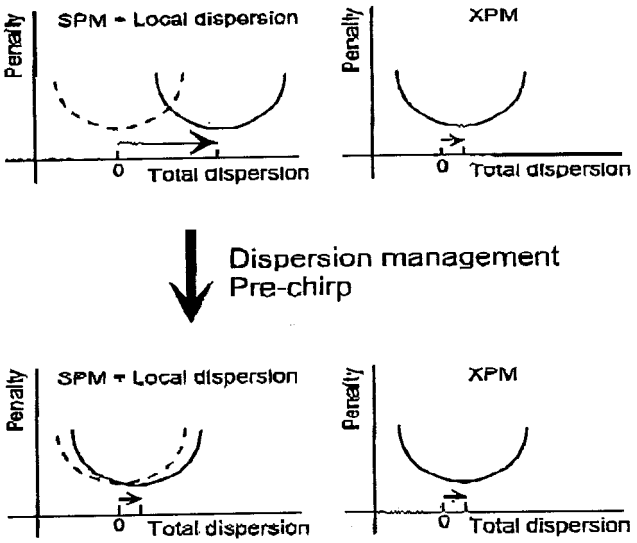

Fig. 1. Dependence of the power penalty, induced by SPM-GVD and XPM-GVD interaction, on the total dispersion at the receiver.

of the transmission line. However, the optimum total dispersion values with regard to SPM-GVD and XPM-GVD interaction deviate from zero as shown in Fig. 1.

In the case of single channel transmission, this deviation arises from the following factors.

1) If the signal is initially chirped, since this initial chirping should be compensated at the receiver, excess dispersion is necessary.
2) SPM induces blue shift chirping during transmission that should also be compensated.
3) SPM is mainly generated near the input end of the fiber ($0 < z < L_{\text{eff}}$). L_{eff} is the effective length of the fiber expressed as [13]

$$L_{\text{eff}} = \frac{1}{a}\{1 - \exp(-aL)\} \tag{1}$$

where a is the attenuation coefficient of the fiber, and L is the length of the fiber. Let us consider the signal propagation by dividing the transmission fiber into two segments ($0 < z \leq L_{\text{eff}}$, and $L_{\text{eff}} < z \leq L$), and suppose that SPM is imposed at $z = L_{\text{eff}}$. In this model, the local dispersion over the effective length does not affect the SPM-induced waveform distortion, and causes only small dispersion-induced waveform distortion. In the following segment, SPM interacts with the dispersion $D(L - L_{\text{eff}})$, where D is the local dispersion of the fiber, and causes significant waveform distortion. This means that the local dispersion of the first segment is not responsible for the SPM-induced waveform distortion. In order to equalize this SPM-induced waveform distortion, the fiber dispersion of the second segment should be compensated. Consequently, the total optimum dispersion for SPM (D_{tot}^{SPM}) follows

$$D_{tot}^{\text{SPM}} \simeq DL_{\text{eff}}. \tag{2}$$

Although the optimum total dispersion at the receiver depends on these factors, it is difficult to find the optimum dispersion by a simple rule of thumb because SPM depends on the signal waveform, which changes with propagation. When the channel rate is as high as 40 Gb/s, precise optimization of the total dispersion is necessary because allowable dispersion becomes very small. Precise optimization of the total dispersion demands the numerical solution of the nonlinear Schrödinger equation (NLSE) as discussed in the next section.

In WDM systems, the transmitted waveform is distorted not only by SPM-GVD interaction but also XPM-GVD interaction. Let us consider two WDM channels co-propagating through a fiber with local dispersion D: One, the interfering channel, consists of isolated rising/falling edges with transition time $\Delta\tau$. The other, the probe channel, has constant intensity. In this case, although the probe channel suffers phase modulation as it propagates through the fiber, the phase modulation responsible for waveform degradation is imposed in the first walk-off length [14] given by

$$L_{wo} = \frac{\Delta\tau}{|D|\Delta\lambda} \tag{3}$$

where $\Delta\lambda$ is the wavelength spacing of the two WDM channels. Therefore, the optimum total dispersion for XPM-GVD interaction deviates from zero in the same way as for SPM. The optimum total dispersion for XPM (D_{tot}^{XPM}), given by

$$D_{tot}^{\text{XPM}} \simeq DL_{wo} = \text{sgn}(D)\frac{\Delta\tau}{\Delta\lambda} \tag{4}$$

is independent of local dispersion. In addition, the XPM penalty is only slightly dependent on the initial chirping and sign of the fiber dispersion [15].

Consequently, the optimum dispersion for SPM-GVD suppression is not, in general, equal to that for XPM-GVD suppression. Moreover, the optimum total dispersion for SPM depends on the prechirping, local dispersion, and the fiber input power. Therefore, by properly setting the prechirping and local dispersion, we can adjust the optimum total dispersion for SPM-GVD to equal that for XPM-GVD. In this condition, the waveform distortion induced by both effects is minimized.

Although the RZ format has better performance at high-fiber input powers [16], we assume, in the following of this paper, the NRZ format for line coding because it facilitates the transmitter configuration and is widely used in current communication systems.

III. Single-Channel Transmission

We will discuss the dependence of single-channel transmission characteristics on prechirping, fiber input power, and local dispersion by the aid of numerical simulations. The system configuration considered in this simulation is shown in Fig. 2(a). The transmitted signal is a single-channel 40-Gb/s NRZ format. The modulator is assumed to be a Mach–Zehnder type having chirp-parameter α. The transmission line consists of four 100-km dispersion-shifted fibers. In order to minimize the interaction of SPM and fiber dispersion, in-line dispersion compensation is used. Taking into account the difficulty of

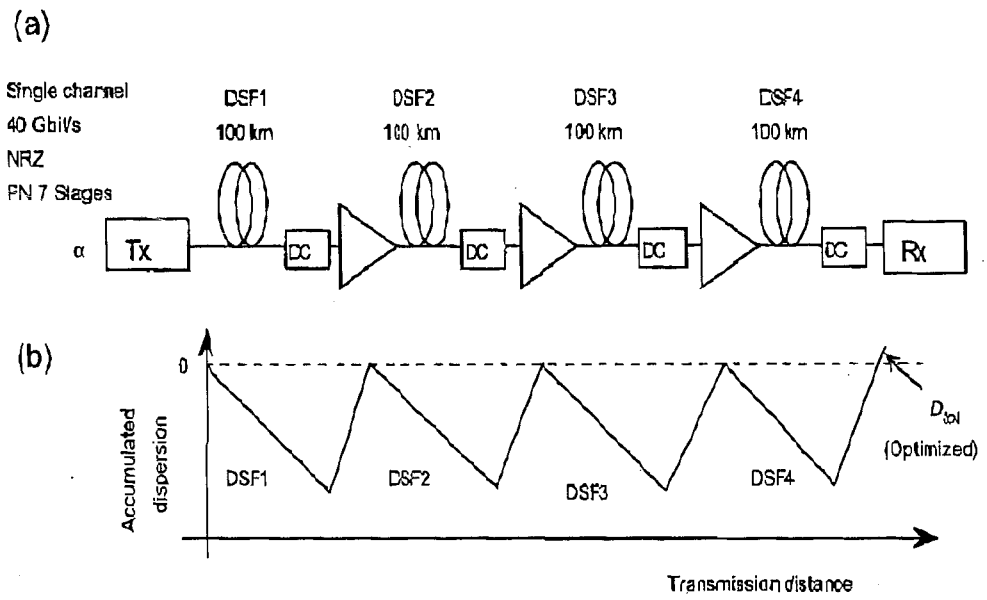

Fig. 2. (a) System configuration and (b) dispersion map of the single-channel transmission simulation.

dispersion optimization in practical field circumstances, the compensation ratio of each span is set to 100%, and the total dispersion D_{tot} is optimized by adding excess dispersion in front of the receiver [Fig. 2(b)]. The transmitted waveform was derived by solving the NLSE using the split-step Fourier (SSF) method. Here we take the attenuation coefficient $a = 0.2$ dB/km, dispersion slope $dD/d\lambda = 0.07$ ps/nm^2/km, and the nonlinear coefficient $\gamma = 2$ W^{-1}km^{-1}. Slope compensation and amplifier spontaneous emission noise are not considered in these simulations.

Fig. 3 shows the contour plot of the calculated 1-dB eye opening penalty (EOP) as a function of local dispersion, accumulated dispersion, and the modulator chirp-parameter α at various fiber input powers. The regions inside the contour lines are the transmission windows at each fiber-input power. At low-fiber input power ($P_{\rm in} = +1, +4$ dBm), the window does not depend on local dispersion, only initial chirping. As the input power increases, however, it starts shrinking because of the SPM-induced chirping and the window depends on both initial chirping and local dispersion. As explained in the previous section, the dependence on local dispersion is given by (2), which is shown by the dashed and double-dotted lines, which is offset from the zero total dispersion at the local dispersion of 0 ps/nm/km because excess positive dispersion is necessary in order to compensate the SPM-induced blue shift chirping. Clear dependence of the window on $DL_{\rm eff}$ is seen at high fiber input powers ($+7$, $+10$ dBm). As for initial chirping, negative (blue shift) or zero chirp is suitable for positive (anomalous) dispersion fibers, while positive (red shift) chirp is suitable for negative (normal) dispersion fibers. We attribute these optimum combinations to the fact that the waveform distortion in the effective length is suppressed by initial chirping that has opposite sign to the dispersion-induced chirping.

These results suggest that we can control the optimum total dispersion of the single-channel transmission by changing the local dispersion of the transmission fiber and the initial chirping.

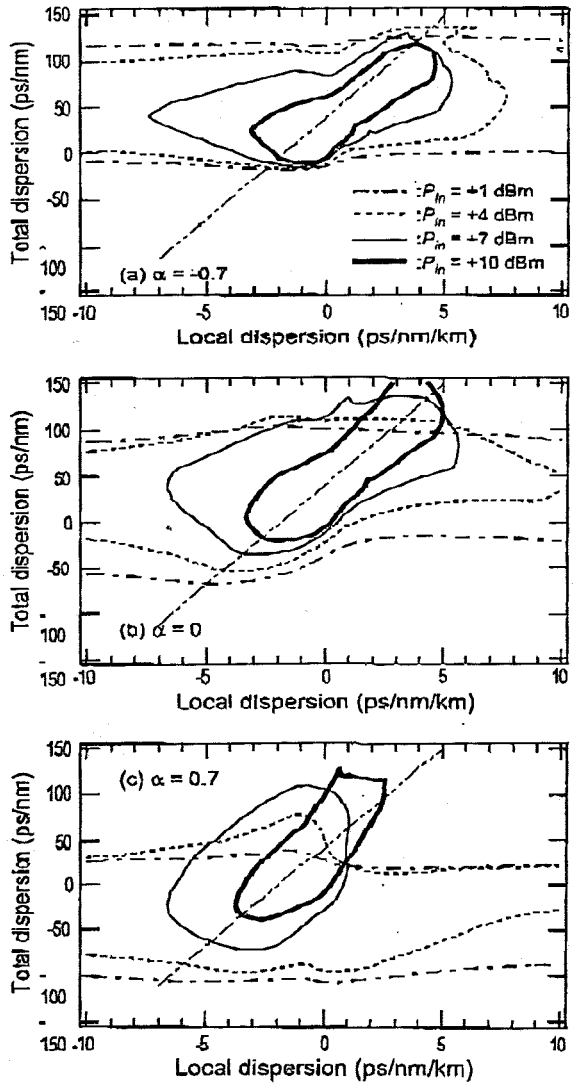

Fig. 3. Contour plots of calculated eye-opening penalty as a function of local dispersion and total dispersion.

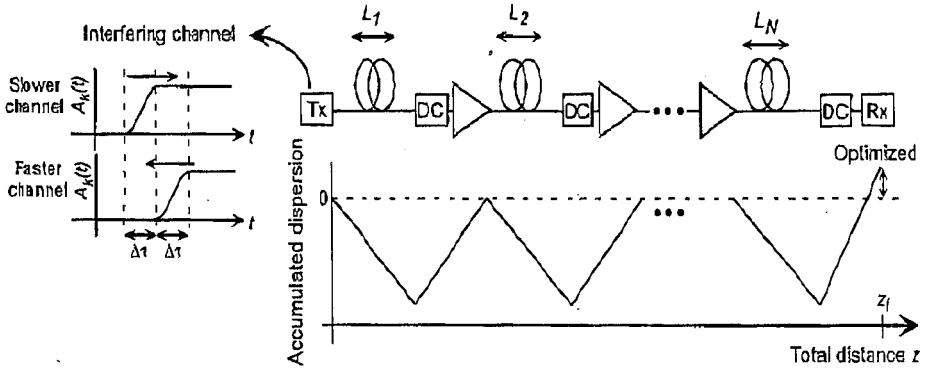

Fig. 4. System configuration and dispersion map of four-channel WDM transmission.

IV. WDM Transmission

A. Analysis of XPM-Induced Power Penalty

When a system is upgraded to handle multiwavelengths, the transmission window evaluated for single-channel systems is restricted by nonlinear interchannel crosstalk effects such as FWM and XPM. Since XPM causes serious degradation in the case of NZDSF transmission, we will evaluate XPM-induced signal distortion in this section. Of course, computer simulation yields good predictions as is true for the single-channel case. However, when designing a WDM system, we must examine various parameters such as channel spacing, channel number, and so on. For this reason, we will take a semi-analytical approach to estimating the XPM-induced penalty and check the obtained results by computer simulation.

There have been several contributions to the analysis of XPM-induced amplitude modulation [14], [15], [17], [18]. We start with a brief summary of the formulation. Neglecting the frequency dependence of the modal distribution on the signal wavelength and omitting the FWM component, the propagation equation for the jth channel of WDM signals is given by

$$\frac{\partial A_j}{\partial z}+\frac{a}{2}A_j+\beta_{1j}\frac{\partial A_j}{\partial t}+\frac{i}{2}\beta_{2j}\frac{\partial^2 A_j}{\partial t^2}+\frac{1}{6}\beta_{3j}\frac{\partial^3 A_j}{\partial t^3} = i\gamma\left(|A_j|^2+2\sum_{k\neq j}|A_k|^2\right) \tag{5}$$

where

A_j	slowly varying envelope of jth channel signal field;
$\beta_{1j}=1/v_{gj}$, v_{gj}	group velocity;
β_{2j} and β_{3j}	quadratic and cubic term in a Taylor series of the propagation constant $\beta_j(\omega)$, respectively.

Let us consider a transmission line with in-line dispersion compensation as shown in Fig. 4. Since the waveform change in the first walk-off length is small, we neglect the dispersion term in (5) for the first approximation. In this condition, the nonlinear phase-shift due to XPM is expressed as

$$\phi_j(z,t)=2\gamma\sum_{m=1}^{N}\sum_{k\neq j}\int_0^{L_m}\cdot|A_k(0,t+d_{jk}z-\Delta t_{jkm})|^2e^{-az}\,dz \tag{6}$$

where d_{jk} is the walk-off parameter

$$d_{jk}=\frac{1}{v_j}-\frac{1}{v_k}\simeq-\left\{D(\lambda_k-\lambda_j)+\frac{1}{2}\frac{dD}{d\lambda}(\lambda_k-\lambda_j)^2\right\} \tag{7}$$

and Δt_{jkm} is the delay of kth channel against the jth channel at the input of mth fiber section

$$\Delta t_{jkm}=\sum_{n=1}^{m-1}\left[\{D_n(L_n-L_{Cn})\}(\lambda_k-\lambda_j)+\frac{1}{2}\left(\frac{dD}{d\lambda}\right)_n L_n(\lambda_k-\lambda_j)^2\right] \tag{8}$$

where L_n is the length of the nth section, and L_{Cn} is the portion of the fiber length whose dispersion is compensated.

In the same way as the previous section, we will consider a dispersion-managed transmission line in which all sections have the same value of local dispersion. In order to evaluate the amplitude modulation generated by PM–AM conversion, the probe channel is assumed to carry a CW signal. We also assume that the total dispersion of the target channel is compensated to zero at the output of each section, and that the total dispersion is optimized in front of the receiver (Fig. 4). In this case, the amplitude modulation at the receiver ($z=z_t$, z_t is the total length of the transmission line) is given by

$$A_j(z_t,t)=\exp[\hat{D}]A_0\exp[i\phi_j(z_t,t)] \tag{9}$$

where the dispersion operator $\hat{D}$ is expressed as

$$\hat{D}=-i\left\{(L_N-L_{CN}-L'_{wo})\frac{\beta_2}{2}\right\}\frac{\partial^2}{\partial t^2}. \tag{10}$$

In general, since there exist various walk-off lengths (L_{wo}) depending on the channel spacing ($|\lambda_k-\lambda_j|$), we introduced the effective walk-off length L'_{wo} in (10). L'_{wo} satisfies $0<L'_{wo}<\Delta\tau/(|D|\Delta\lambda)$, where $\Delta\lambda$ is the minimum wavelength spacing, but we took $L'_{wo}=\Delta\tau/(|D|\Delta\lambda)$ because the nearest channel causes the most severe phase shift.

In addition to amplitude modulation, we estimated the timing jitter. From the frequency chirping given by

$$\Delta f(z,t)=\frac{1}{2\pi}\frac{\partial}{\partial t}\phi_j(z,t) \tag{11}$$

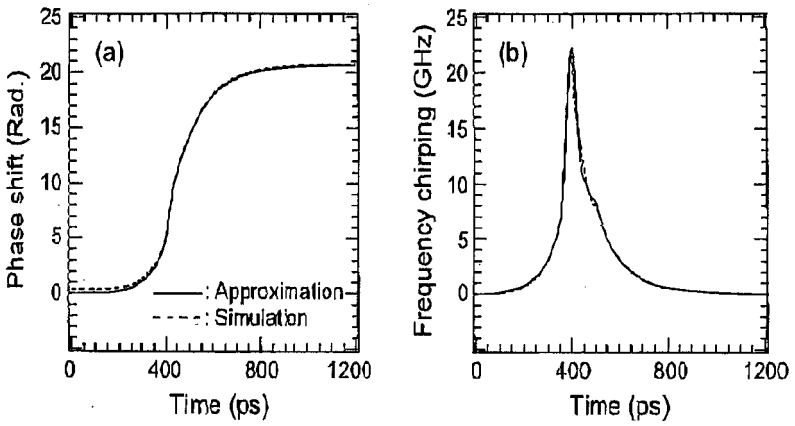

(a) (b)

Fig. 5. Calculated XPM-induced phase shift (a) and frequency chirping (b).

we calculated the timing jitter by averaging the frequency chirping over one time slot T_b,

$$\Delta\tau_i(z_t, t) \simeq \frac{\lambda_j^2}{c} D(L_N - L_{CN} - L'_{wo}) \frac{1}{T_b} \int_t^{t+T_b} \Delta f(z_t, t')\, dt'. \tag{12}$$

B. Calculation Results

Let us consider a four-channel WDM system as one example. Taking account of the high spectral efficiency, 100-GHz spacing has been investigated by using Raman amplification technique in 40-Gb/s/ch systems [3], [5]. In this calculation, however, the channel spacing was set to 200 GHz because FWM penalty is dominant in 100-GHz spaced system when fiber input power is as high as $+10$ dBm. We will examine the transmission characteristics of the second channel from the shortest wavelength channel (λ_2). The waveform of the interfering channels was an isolated leading/falling edge with $\Delta\tau = 25$ ps which corresponds to a 40-Gb/s NRZ format. In order to estimate the worst-case for XPM-induced timing jitter, the timing of the channels with faster group velocity was delayed by $\Delta\tau$ from the edge of the channels with slower group velocity, as shown in Fig. 4 (As for amplitude modulation, the worst case relative timing is different from this case). The configuration of the transmission line and the fiber parameters were the same as in the previous section: Total length $= 4 \times 100$ km, $a = 0.2$ dB/km, $dD/d\lambda = 0.07$ ps/nm^2/km, and $\gamma = 2$ W^{-1}km^{-1}.

Fig. 5 compares the phase shift and frequency chirping of λ_2 as calculated by numerical simulation using SSF method and by the approximation. Here the input peak power for each channel was $+13$ dBm/ch ($+10$ dBm/ch in average), and the local dispersion was 2 ps/nm/km. The waveform obtained from the approximation is confirmed to agree well with the simulation results.

Fig. 6 shows the contour plot of calculated power penalty induced by PM-AM conversion [Fig. 6(a)] and that of timing jitter [Fig. 6(b)] calculated for CH 2 as a function of the local dispersion and the total dispersion, where the power penalty is defined as the ratio of the minimum intensity calculated from to the intensity without XPM (power penalty $= \min[|A_j|^2]/|A_0|^2$).

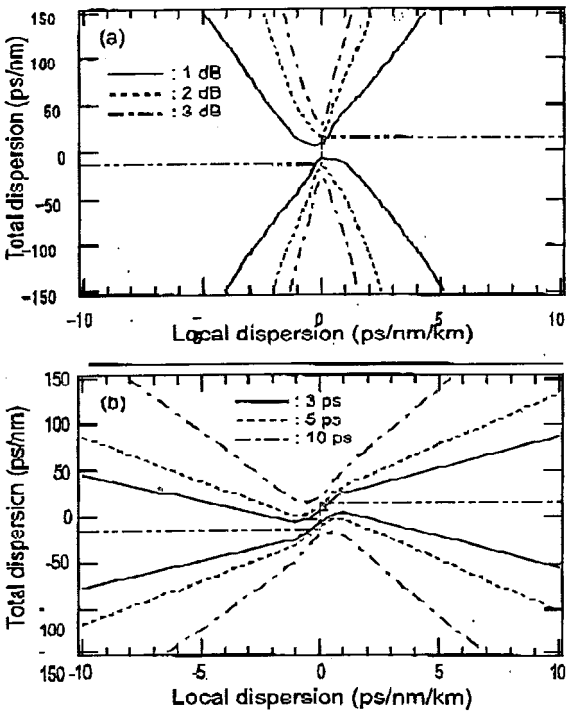

Fig. 6. Contour plots of calculated XPM-induced power penalty and timing jitter. (a) Power penalty due to amplitude modulation. (b) Timing jitter.

Since Fig. 6(a) is the results for the worst case for timing jitter, the power penalty would be larger than Fig. 6(a) when the relative timing between the channels is set to the worst case for amplitude distortion. In our calculation, the average fiber input power was set to $+10$ dBm/ch, and we assumed that the dispersion of the prove channel (CH 2) is compensated to zero-dispersion at the output of the each section, and the total dispersion is changed by adding the excess dispersion in front of the receiver, as shown in Fig. 4. The dispersion slope compensation is not considered in this calculation. The optimum dispersion given by (4), shown by the dashed and double-dotted lines, does not depend on the magnitude of the local dispersion but only depends on the sign of the local dispersion (Although the optimum total dispersion appears to be dependent on the local dispersion around the zero-local dispersion, this is caused by the

software problem plotting the contour line. Besides, the transmission performance is limited by FWM at these regions). As the total dispersion deviates from this value, both power penalty and the timing jitter increases. Moreover, as the local dispersion deviates from zero, the transmission window extends both for power penalty and timing jitter. So the high local dispersion is effective in order to suppress the XPM-induced power penalty and timing jitter. (However, as the local dispersion increases, the transmission performance is limited by SPM-GVD interaction, as shown in Fig. 3.) Since about 3.25 ps timing jitter (13% of the bit period) results in 1 dB power penalty when Gaussian distribution is assumed [19], we take this value as the allowable timing jitter, as shown by solid line in Fig. 6(b). (Here the power penalty is lower than 1 dB because the calculation result shows the worst case timing jitter.) From Fig. 6, it is clear that the fiber input power is restricted mainly by the timing jitter due to XPM-induced chirping when the bit rate approaches 40 Gb/s. It should be noted, moreover, that the amplitude modulation decreases rapidly compared to timing jitter as the local dispersion deviates from zero.

The transmission window is the area common to these windows [Fig. 6(top) and (bottom)] and the single channel transmission window (Fig. 3). Fig. 7 shows these three contour plots for 4-ch WDM transmission over 4×100 km fiber with the average fiber input power of $+10$ dBm/ch and the channel spacing of 200 GHz. There is only a small common area when $\alpha = -0.7$ [Fig. 7(a)] or 0. [Fig. 7(b)]. This means that it is difficult to fully suppress the SPM-induced power penalty and XPM-induced power penalty at the same time. In the case of $\alpha = 0.7$ [Fig. 7(c)], on the other hand, there exists a wide transmission window (shown by the hatched area) when the local dispersion is negative. Consequently, by using red shift prechirping and normal dispersion fibers, we can improve the allowable fiber input power.

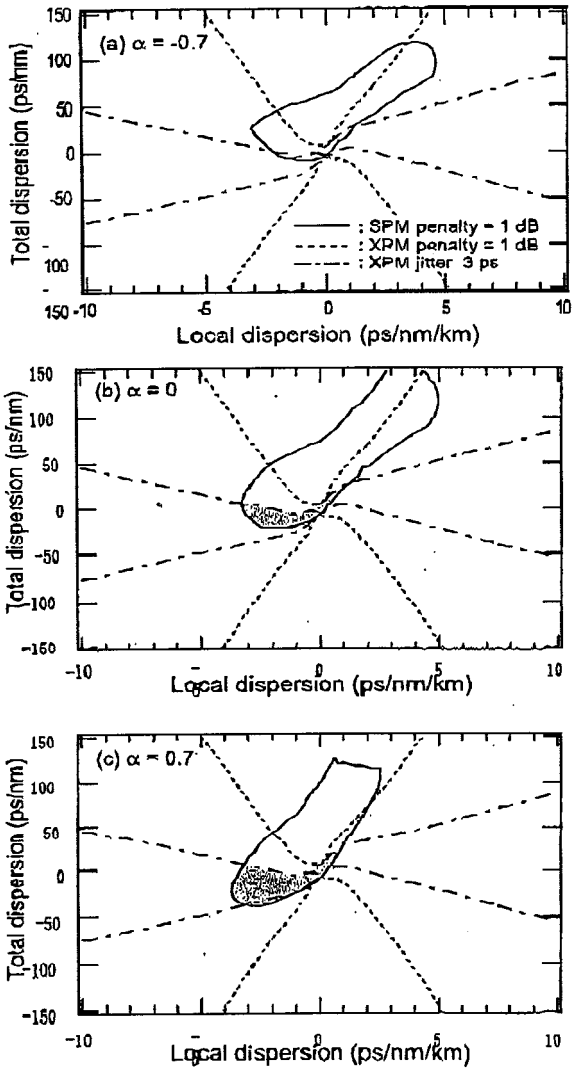

Fig. 7. Contour plots of (a) calculated SPM-induced eye-opening penalty, (b) XPM-induced eye-opening penalty, and (c) XPM-induced timing jitter.

C. Numerical Simulation Using Split-Step Fourier Method

In order to confirm these results, we performed 4-ch WDM simulation using the SSF method for two cases.

Case A) $D = 2$ ps/nm/km, $D_{tot} = 70$ ps/nm, and $\alpha = -0.7$.

Case B) $D = -2$ ps/nm/km, $D_{tot} = -20$ ps/nm, and $\alpha = 0.7$.

The same fiber parameters as in the previous sub-section were used in this simulation. In this simulation, each channel was modulated by a $2^7 - 1$ pseudorandom bit sequence (PRBS), where each sequence was shifted by a quarter period from the sequence of the neighboring channel. Fig. 8 shows the obtained optical eye patterns before and after transmission for CH 2. The eye for Case B) [Fig. 8(b)] has clear eye openings, but the eye for Case A) [Fig. 8(bottom)] shows severe timing jitter and amplitude modulation. These results agree well with the previous discussion.

V. 4×40 Gb/s Transmission Experiment

A. Experimental Setup

A 4×40 Gb/s transmission experiment was performed in order to confirm the effect of prechirping and dispersion management. The experimental setup is shown in Fig. 9. A prototype transmitter based on high-speed InP HEMT digital IC technology was used [20]. Taking account of relatively small local dispersion of the transmission fiber used in the experiment (-1.5 and $+1.6$ ps/nm/km), the signal wavelengths were separated by 250 GHz ($\lambda_1 = 1549.9$ nm, $\lambda_2 = 1551.9$ nm, $\lambda_3 = 1553.9$ nm, $\lambda_4 = 1555.9$ nm). 40 Gb/s NRZ signals ($2^7 - 1$ PRBS) were generated by using a $LiNbO_3$ Mach–Zehnder modulator with a low driving voltage of 3.0 V [21]. The chirp parameter, α, was controlled by changing the dc bias voltage of the $LiNbO_3$ modulator. The modulated signals were decorrelated by 20-ps/nm dispersion fibers. The transmission line consisted of $4\times$ 100-km NZDSF with either positive or negative dispersion. Two combinations of α and local dispersion D were tested.

Case 1) $\alpha < 0$, and $D = +1.6$ ps/nm/km.

Case 2) $\alpha > 0$, and $D = -1.5$ ps/nm/km.

The average zero-dispersion wavelength of each section was adjusted to $\sim$1552 nm ($\simeq \lambda_2$) by using high-dispersion fibers (HDF; conventional dispersion-compensating fibers (DCF) for negative dispersion, SMF for positive dispersion), but the dis-

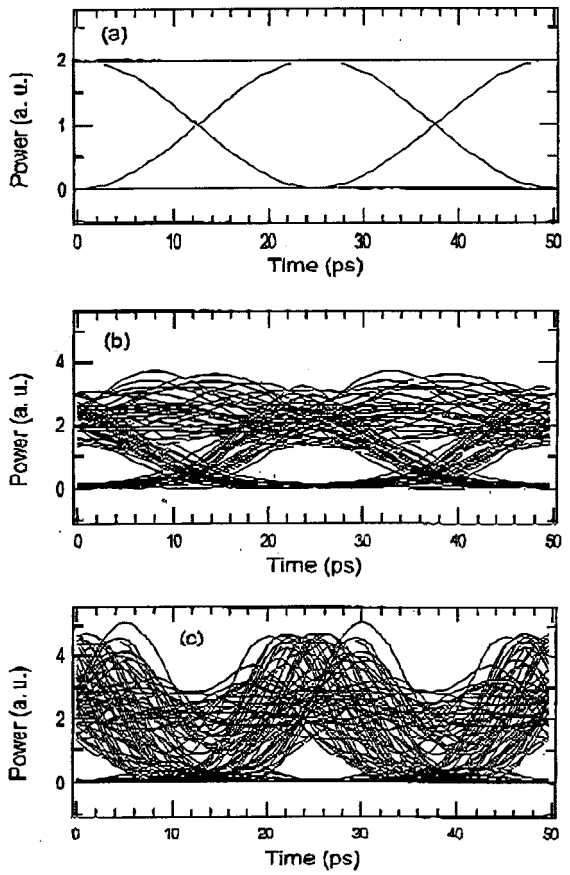

Fig. 8. Calculated eye diagrams with 4×40-Gb/s, 400-km transmission. (a) Before transmission. (b) After transmission. $\alpha = 0.7$, $D = -2$ ps/nm/km, $D_{tot} = -20$ ps/nm. (c) After transmission. $\alpha = -0.7$, $D = 2$ ps/nm/km, $D_{tot} = 70$ ps/nm.

persion slope was not compensated in this experiment. The average power at the input of each section was +10 dBm/ch. At the receiver side, the total dispersion for each channel was optimized by using HDF, and the transmitted signal was wavelength-division demultiplexed by a 1-nm optical bandpass filter, time-division demultiplexed by a polarization-insensitive EA modulator, and electrically demultiplexed to 10 Gb/s and fed into an error detector.

B. Experimental Results

Fig. 10 shows the measured eye diagrams for λ_2 of single-channel and WDM transmission. The accumulated dispersion was optimized to +50 in Case 1) and 0 ps/nm in Case 2). In both cases, the eye diagrams for single channel transmission exhibited clear eye openings [Fig. 10(b) and (d)]. In the case of WDM transmission, however, the eye in Case 1) was closed due to the timing jitter induced by the interaction between XPM and accumulated dispersion [Fig. 10(c)]. On the contrary, the combination of negative dispersion and positive initial chirp suppressed this timing jitter and clear eye opening was obtained [Fig. 10(e)].

The measured optical spectra before and after transmission are shown in Fig. 11. Since the ratios of the FWM components to the transmitted signal are about 25 dB, the FWM-induced penalties were small in both cases. Spectral broadening caused by SPM was observed, and the spectral widths differed slightly channel-by-channel. These differences in spectral widths are due to the waveform differences at the output of each section caused by the residual dispersion due to the dispersion slope of the transmission line.

Fig. 12 shows measured bit error rate (BER) characteristics for back-to-back and 400-km transmission [Case 2)]. The accumulated dispersion for each WDM channel was optimized individually by changing the dispersion of the DCF in front of the receiver. The measured sensitivities at the BER of 10^{-9} ranged from -28.1 (λ_2) to -26.9 dBm (λ_1) for back-to back, and -26.0 (λ_2) to -21.9 dBm (λ_4) for 400-km transmission. In both cases, error free operation (BER better than 10^{-11}) was confirmed. In Case 1), on the other hand, stable bit error rate measurements were not possible because timing extraction failed due to XPM-induced timing jitter. The power penalties in Case 2), 2.1 (λ_2) to 5.9 dB (λ_4), were caused by the FWM and weak XPM-induced timing jitter. This timing jitter was not suppressed completely because of the residual dispersion at the output of each section due to the dispersion slope of the transmission fiber: Since the accumulated dispersion slope per section is about 7 ps^2/nm, the accumulated dispersions per section due to the dispersion slope ranged from -14 (λ_1) to 28 ps/nm (λ_4). Note that the residual dispersion slope shifts the relative timing between the channels, and the XPM-induced timing jitter is somewhat relaxed because of this timing shift. The application of the inline dispersion slope compensation reduces the residual dispersion at the output of each section on the one hand, but causes realignment of the relative timing between the channels on the other hand. Therefore, in addition to the dispersion slope compensation, the technique that shifts the relative timing between the channels in the transmission line is important in order to suppress the XPM-induced power penalty and timing jitter [22]–[24].

VI. Conclusion

We have examined the dependence of the optimum total dispersion on prechirping, local dispersion and fiber input power in 40-Gb/s/ch WDM transmission systems based on NZDSF by numerical simulations and semi-analytical calculations. The optimum total dispersion for SPM-GVD interaction was shown to deviate, in general, from that for XPM-GVD interaction. Although the optimum dispersion for XPM-GVD interaction has only a small dependence on prechirping and local dispersion, that for SPM-GVD interaction is sensitive to all of them. The difference in local dispersion dependence occurs because the effective length is independent of the local dispersion Eq. (1), while the walk-off length is inversely proportional to it Eq. (3). The optimum dispersion values for SPM-GVD and XPM-GVD can be made to match by combining red shift chirping and negative dispersion fibers. This yielded the highest input power without waveform degradation. An XPM-induced penalty estimation showed that transmission performance of high bit rate WDM systems is severely restricted by timing jitter, which is not so serious in lower bit rate systems. In our theoretical analysis, the effective length is supposed to be independent on the local dispersion. This is valid when the waveform change within the effective length is small. In highly dispersive systems such

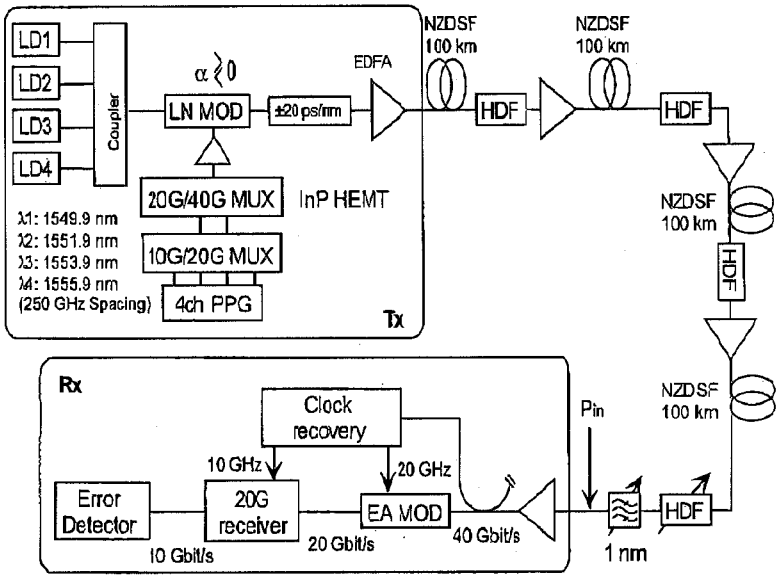

Fig. 9. Experimental setup.

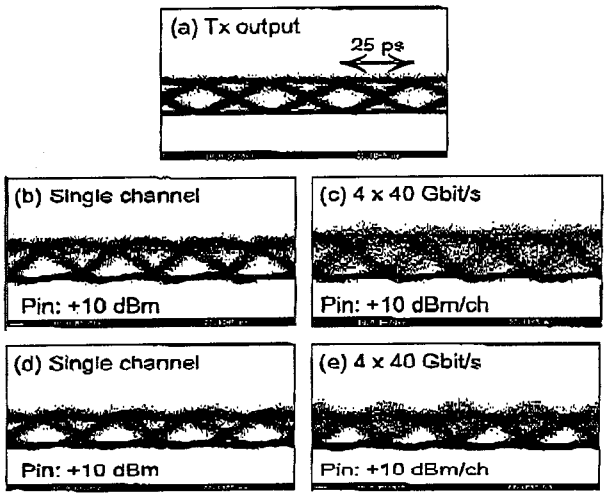

Fig. 10. Measured eye diagrams. (a) Before transmission. (b) After single-channel transmission. $\alpha < 0$, $D = 1.6$ ps/nm/km, $D_{tot} = 50$ ps/nm. (c) After 4 channel transmission. $\alpha < 0$, $D = 1.6$ ps/nm/km, $D_{tot} = 50$ ps/nm. (d)After single-channel transmission. $\alpha > 0$, $D = -1.5$ ps/nm/km, $D_{tot} = 0$ ps/nm. (e) After 4 channel transmission. $\alpha > 0$, $D = -1.5$ ps/nm/km, $D_{tot} = 0$ ps/nm.

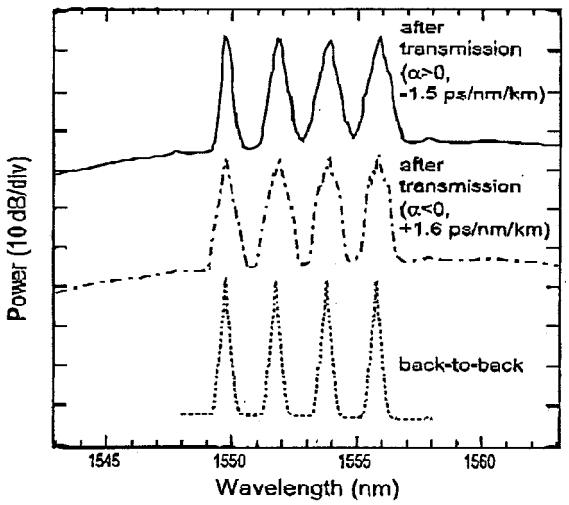

Fig. 11. Measured optical spectra.

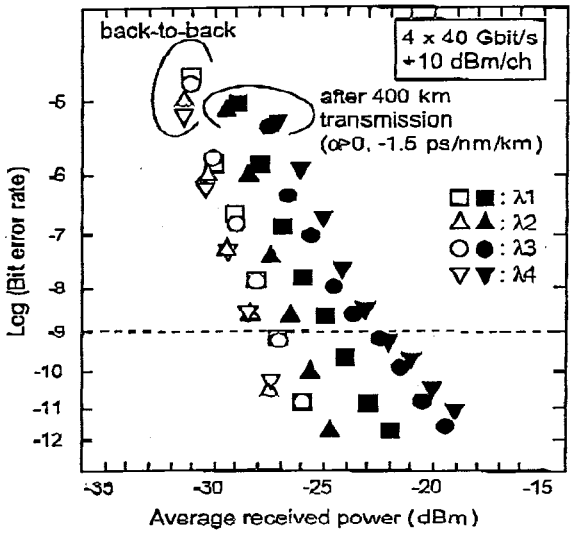

Fig. 12. Measured BER characteristics.

as picosecond pulse transmission over SMF, however, the signal pulse broadens immediately at the input of the fiber because of the fiber dispersion. In these systems, we believe that the dependence of the effective length on the local dispersion should be taken into account.

The calculated results were confirmed in a 4× 40 Gb/s WDM transmission experiment. By using red shift prechirping and negative dispersion fibers, 4× 100 km transmission was successfully demonstrated at the average fiber input power of +10 dBm/ch. In this experiment, however, channel-dependence of the optical spectrum and that of the bit error rate characteristics, caused by the residual dispersion due to the dispersion slope of the transmission fiber, was observed. Therefore in-line dispersion slope compensation will be necessary in order to transmit a number of channels at such high input powers. In addition, the

technique that shifts the relative timing between the channels in the transmission line is important in order to avoid the increase in XPM-induced power penalty and timing jitter caused by the realignment of the relative timing.

ACKNOWLEDGMENT

The authors thank M. Kawachi and K. Sato for their encouragement, M. Yoneyama for fruitful discussions, and K. Noguchi for providing the high-speed $LiNbO_3$ modulator.

REFERENCES

[1] K. Hagimoto, Y. Miyamoto, and Y. Yamabayashi, "40-Gbit/s transmission systems," in *Proc. OFC'98*, 1998, paper WC3.

[2] E. Lach, M. Kaiser, W. Pöhlmann, and G. Vaith, "40 Gbit/s ETDM binary NRZ transmission over installed G.652 field fiber with enhanced dispersion tolerance," in *Proc. ECOC'99*, vol. 2, 1999, pp. 86–87.

[3] R. Ohira, Y. Yano, A. Noda, Y. Suzuki, C. Kurioka, M. Tachigori, S. Moribayashi, K. Fukuchi, T. Ono, and T. Suzaki, "40 Gbit/s × 8-ch NRZ WDM transmission experiment over 80 km × 5-span using distributed Raman amplification in RDF," in *Proc. ECOC'99*, vol. 2, 1999, pp. 176–177.

[4] Y. Zhu, W. S. Lee, G. Pettitt, M. Jones, and A. Hajifotiou, "Eight-channel 40 Gb/s RZ transmission over four 80 km spans (328 km) of NDSF with a net dispersion tolerance in excess of 180 ps/nm," in *Proc. OFC2000*, 2000, paper TuD4.

[5] T. N. Nielsen, A. J. Stentz, P. B. Hansen, Z. J. Chen, D. S. Vengsarkar, T. A. Strasser, K. Rottwitt, J. H. Park, S. Stulz, S. Cabot, K. S. Feder, P. S. Westbrook, and S. G. Kosinski, "1.6 Tb/s (40×40 Gb/s) transmission over 4×100 km nonzero-dispersion fiber using hybrid Raman/Erbium-doped inline amplifiers," in *Proc. ECOC'99*, 1999, paper PD2-2.

[6] J.-P. Elbers, C. Scheerer, A. Färbert, C. Glingener, A. Schöpflin, E. Gottwald, and G. Fischer, "3.2 Tbit/s (80×40 Gbit/s) bi-directional DWDM/ETDM transmission," in *Proc. ECOC'99*, 1999, paper PD2-5.

[7] Y. Miyamoto, K. Yonenaga, S. Kuwahara, M. Tomizawa, A. Hirano, H. Toba, K. Murata, Y. Tada, Y. Umeda, and H. Miyazawa, "1.2-Tbit/s (30×42.7-Gbit/s ETDM optical channel) WDM transmission over 376 km with 125-km spacing using forward error correction and carrier-suppressed RZ format," in *Proc. OFC2000*, 2000, paper PD26.

[8] M. Eiselt, L. D. Garret, and R. W. Tkach, "Experimental comparison of WDM system capacity in conventional and nonzero dispersion shifted fiber," *IEEE Photon. Technol. Lett.*, vol. 11, pp. 281–283, 1999.

[9] A. Bertaina, S. Bigo, C. Francia, S. Gauchard, J.-P. Hamaide, and M. W. Chbat, "Experimental investigation of dispersion management for an 8×10-Gb/s WDM transmission over nonzero dispersion-shifted fiber," *IEEE Photon. Technol. Lett.*, vol. 11, pp. 1045–1047, 1999.

[10] A. Sano, Y. Miyamoto, T. Kataoka, H. Kawakami, and K. Hagimoto, "10 Gbit/s, 300 km repeaterless transmission with SBS suppression by the use of the RZ format," *Electron. Lett.*, vol. 30, pp. 1694–1695, 1994.

[11] N. S. Bergano, C. R. Davidson, and F. Heismann, "Bit synchronous polarization and phase modulation scheme for improving the performance of optical amplifier transmission systems," *Electron. Lett.*, vol. 32, pp. 52–54, 1996.

[12] T. Georges, "Extended path-averaged soliton regime in highly dispersive fibers," *Opt. Lett.*, vol. 22, pp. 679–681, 1997.

[13] G. P. Agrawal, *Nonlinear Fiber Optics*, 2nd ed. San Diego, CA: Academic, 1995.

[14] M. Shtaif, "Analytical description of cross-phase modulation in dispersive optical fibers," *Opt. Lett.*, vol. 23, pp. 1191–1193, 1998.

[15] N. Kikuchi, K. Sekine, and S. Sasaki, "Analysis of cross-phase modulation (XPM) effect on WDM transmission performance," *Electron. Lett.*, vol. 33, pp. 653–654, 1997.

[16] D. Breuer and K. Petermann, "Comparison of NRZ-and RZ-modulation format for 40-Gb/s TDM standard-fiber systems," *IEEE Photon. Technol. Lett.*, vol. 9, pp. 398–400, 1997.

[17] T.-K. Chiang, N. Kagi, T. K. Fong, M. E. Marhic, and L. G. Kazovsky, "Cross-phase modulation in dispersive fibers: Theoretical and experimental investigation of the impact of modulation frequency," *IEEE Photon. Technol. Lett.*, vol. 6, pp. 733–736, 1994.

[18] A. V. T. Cartaxo, "Cross-phase modulation in intensity modulation-direct detection WDM systems with multiple optical amplifiers and dispersion compensators," *J. Lightwave Technol.*, vol. 17, pp. 178–190, 1999.

[19] G. P. Agrawal, *Fiber-Optic Communication Systems*, 2nd ed. New York: Wiley, 1997.

[20] M. Yoneyama, Y. Miyamoto, T. Otsuji, A. Hirano, H. Kikuchi, T. Ishibashi, and H. Miyazawa, "Fully electrical 40-Gbit/s TDM system prototype and its application to 160-Gbit/s WDM transmission," in *Proc. OFC'99*, 1999, paper ThI6.

[21] K. Noguchi, O. Mitomi, and H. Miyazawa, "Millimeter-wave Ti:$LiNbO_3$ optical modulators," *J Lightwave Technol.*, vol. 16, pp. 615–619, 1998.

[22] M. Eiselt, "Does spectrally periodic dispersion compensation reduce nonlinear effects?," *Proc. ECOC'99*, vol. 1, pp. 144–145, 1999.

[23] G. Belloti and S. Bigo, "Cross-phase modulation suppressor for multi-span dispersion-managed WDM transmission," in *Proc. ECOC'99*, vol. 1, 1999, pp. 204–205.

[24] A. Hirano, K. Yonenaga, Y. Miyamoto, H. Toba, H. Takenouchi, and H. Tsuda, "640-Gbit/s (16-ch × 42.7 Gbit/s) WDM L-band DSF transmission with 25-nm bandwidth slope compensator," in *ECOC 2000*, 2000, Paper 10.1.2.

Akihide Sano, photogrpah and biography not available at the time of publication.

Yutaka Miyamoto (M'93), photogrpah and biography not available at the time of publication.

Shoichiro Kuwahara, photogrpah and biography not available at the time of publication.

Hiromu Toba (M'91), photogrpah and biography not available at the time of publication.